


RESEARCH

Open Access



# Molecular characterization of a novel polerovirus from bitter melon plants and dynamic subcellular localization of the virus-encoded proteins

Rui Qiao<sup>1,2†</sup>, Linhao Ge<sup>2†</sup>, Mengjiao Pan<sup>1,2</sup>, Shoulin Jiang<sup>1,2</sup>, Jieyin Chen<sup>2</sup>, Wenxing Liang<sup>1\*</sup>, Xueping Zhou<sup>2,3\*</sup> and Fangfang Li<sup>1,2\*</sup> 

## Abstract

Viruses within the *Polerovirus* genus in the family of *Solemoviridae* have a single-stranded positive-sense RNA genome of about 5.6–6.2 kb in length. In this study, the bitter melon leaves showing yellowing and crumple symptoms were collected for small RNAs (sRNAs) sequencing. Analysis of the contigs de novo assembled from sRNA-sequencing data, followed by RT-PCR and cloning, determined the complete viral genome to be 5665 nucleotides. This virus isolate contains conserved ORF3a, ORF3, ORF4, and other typical features of poleroviruses. The P0 protein of this virus isolate shares less than 74.80% amino acid sequence identity with any of the previously characterized poleroviruses, indicating that it should be a novel polerovirus. We name this virus as bitter melon yellowing crumple virus (BYCV). We further revealed the dynamic subcellular localization and protein accumulation of seven proteins encoded by BYCV in *Nicotiana benthamiana* plants over time, and these viral proteins displayed specific subcellular localization. Expressing the BYCV P0 protein using a potato virus X vector caused severe symptoms in *N. benthamiana* plants, while P0 exhibited weak RNA silencing suppression activity. These findings provide an example for investigating the dynamic subcellular localizations of viral proteins and demonstrate that P0 is a critical protein potentially playing an important role in virus infection.

**Keywords** A novel polerovirus, Bitter melon yellowing crumple virus, Dynamic subcellular localization, Silencing suppression activity

<sup>†</sup>Rui Qiao and Linhao Ge contributed equally to this article.

\*Correspondence:

Wenxing Liang  
wliang1@qau.edu.cn  
Xueping Zhou  
zzhou@zju.edu.cn  
Fangfang Li  
lifangfang@caas.cn

<sup>1</sup> Key Lab of Integrated Crop Pest Management of Shandong Province, College of Plant Health and Medicine, Qingdao Agricultural University, Qingdao 266109, China

<sup>2</sup> State Key Laboratory for Biology of Plant Diseases and Insect Pests, Institute of Plant Protection, Chinese Academy of Agricultural Sciences, Beijing 100193, China

<sup>3</sup> State Key Laboratory of Rice Biology, Institute of Biotechnology, Zhejiang University, Hangzhou 310058, China



## Background

Infection by plant viruses can cause severe yield and quality losses in many economically important crops. As important pathogens of plant diseases, plant viruses can be classified into the following types based on their genome features. *Solemoviridae* is a typical family of viruses with a genome of positive single-stranded RNA (+ssRNA) and currently includes four genera (*Enamovirus*, *Polemovirus*, *Polerovirus*, and *Sobemovirus*) (Walker et al. 2021). The diversity of transmission modes in the family *Solemoviridae* significantly promotes viral infectivity, including mechanical wounding, vegetative propagation, soil transmission, and insect vector transmission. *Polerovirus* is currently the largest genus in *Solemoviridae*, with over 20 virus species. This genus belonged to the demolished family of Luteoviridae in the past.

Viruses within the *Polerovirus* genus have a +ssRNA genome of about 5.6–6.2 kb in length, comprising mostly 7 (8 for *Potato leafroll virus*, PLRV) open reading frames (ORFs), without a poly(A) tract at the 3′-terminus. Except for these ORFs (ORF0, ORF1, ORF1-2, ORF3, ORF3a, ORF4, ORF3-5, and an additional ORF 8 for PLRV), the genome of poleroviruses also contain untranslated regions (UTRs), namely 5′ UTR, 3′ UTR (Miller et al. 1995). Like most viruses, poleroviruses encode various proteins with multiple functions. P0 encoded by ORF0, as an RNA-silencing suppressor (RSS), is a notable feature for poleroviruses (Csorba et al. 2010). A VPg released from the P1 polyprotein is connected to the 5′ end of the viral genome (Wilk et al. 1997; Delfosse et al. 2021). The RNA-directed RNA polymerase (RdRP) encoded by ORF2 is expressed as a fusion protein, through a −1 ribosomal frameshift strategy (Koonin and Dolja 1993). P3 encoded by ORF3, circa 22–23 kDa, is a coat protein (CP) which plays a significant role in forming viral particles, movement, and vector transmission (Sömera et al. 2015). ORF4 embedded within ORF3 encodes a movement protein (MP) for viral cell-to-cell movement. Interestingly, the ORF3a located between the promoter of ORF3 and ORF4, possesses a non-AUG codon, and the encoded protein P3a localizes at the Golgi apparatus and plasmodesmata. Therefore, long-distance viral movement mainly depends on P3a. Viral or plasmid vectors can provide P3a in trans to regain the movement function (Smirnova et al. 2015). However, *Enamovirus* is a closely related genus to *Polerovirus*, but viruses in this genus lack P3a and MP (Silva et al. 2017). In addition, ORF3 fused with ORF5 forms a fusion protein, CP-read-through. This read-through protein is expressed starting at the AUG of ORF3 to the whole domain of ORF5 rather than stopping at the end of ORF3 (Xu et al. 2018). The read-through protein regulates aphid transmission and viral limitation in the phloem (Wang et al. 1995). Of

note, variations of poleroviral proteins can interfere with viral resistance and susceptibility genes (Latourrette et al. 2021).

Many important cash crops, including cotton, maize, tobacco, broad bean, pea, and pumpkin, are infected by poleroviruses in the field (Tan et al. 2021). Poleroviruses infect more than 150 plant species in over 20 families, including Solanaceae, Amaranthaceae, and Cruciferae (Mayo et al. 2020). Among different hosts, crops in the family Cruciferae are deeply impaired by poleroviruses. The bitter melon (*Momordica charantia* L.) is a crop in the family Cucurbitaceae. It has been reported that several poleroviruses have been detected on bitter melon plants, including Cucurbit aphid-borne yellows virus (CABYV) and Suakwa aphid-borne yellows virus (SABYV) (Xiang et al. 2008; Shang et al. 2009).

Here we have identified and characterized a novel virus infecting bitter melon using high-throughput sequencing of small RNAs (sRNAs). The viral genome is 5665 nucleotides long and shares the highest nucleotide sequence identity, 79.80% with CABYV. We provided sufficient evidence that the virus belongs to the genus *Polerovirus* based on similar genome features with poleroviruses. Furthermore, the dynamic subcellular localization and accumulation of seven viral proteins encoded by this virus in *Nicotiana benthamiana* plants over time were investigated. In addition, the P0 protein was also confirmed in this study as a pathogenicity factor and an RNA silencing suppressor.

## Results

### Analysis of the sRNAs library and identification of the virus in the bitter melon by De novo assembly of sRNAs

Many bitter melon plants showing yellowing and crumple symptoms were observed in the field of Haikou, Hainan province of China, in January 2021 (Fig. 1a–c). The representative yellowing and crumple leaves were collected, and the total RNA from these samples was extracted. The small RNAs (sRNAs) were further separated and enriched to construct the sRNA library for high-throughput sequencing using Illumina HiSeq 2000/2500 platform (Lianchuan, Beijing, China). As a result, a total of 11,394,826 raw reads were obtained by sequencing. The 3′ adaptor sequences from the original sequencing data were removed first, and the sequences with base lengths less than 15 nt and more than 40 nt were removed. After filtering out the junk sequences, 3,648,114 clean reads were kept. The clean reads were compared to the data with mRNA, Rfam, and Repbase databases, and 2,953,377 valid reads were finally obtained. The lengths of these 2,953,377 sRNAs were mainly concentrated in 18–25 nt (Fig. 1d). Based on the analyzed results, 24 nt sRNAs were the most abundant, accounting for 35.19%

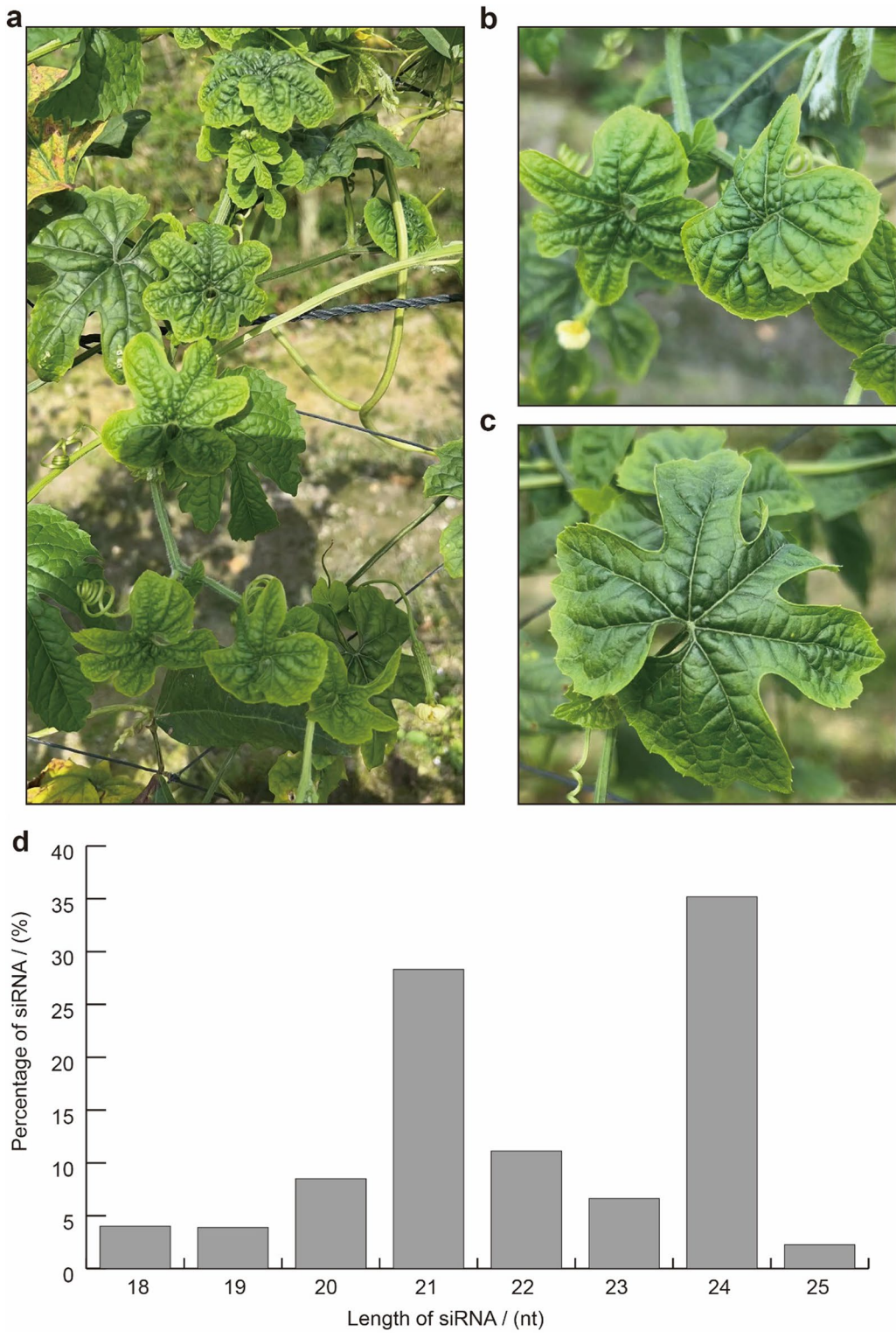


**Fig. 1** Symptoms of virus-infected bitter melon plants collected from the Hainan Province of China. **a** Symptoms on whole bitter melon plants. **b, c** A close view of the symptoms of diseased bitter melon leaves. **d** Length distribution of small RNA sequences

of the total number of sRNAs. A total of 1299 contigs of sRNAs-derived viruses were assembled by the software Velvet Assembler 1.2.10 with parameters k-mer value of 15. BLASTn analysis of the assembled contigs against the NCBI databases resulted in 35 contigs highly similar to CABYV (GenBank accession number NC\_003688) (genus *Polerovirus*, family *Solemoviridae*).

### The complete nucleotide sequence and genome organization of a novel RNA virus

In order to obtain the full-length viral genome sequences, six products of RT-PCR reactions were amplified using specific primers (Additional file 1: Table S1) designed based on the contig sequences. After molecular cloning and sequencing, the complete genome of this virus was determined to be 5665 nt in length (GenBank accession Number: OQ448155). The BLASTn search of the full-length nucleotide sequence against the NCBI database indicated that it had a high identity with the CABYV, belonging to the genus *Polerovirus* of the family *Solemoviridae*, which shares 79.80% nucleotide identity with CABYV. The species demarcation criterion for the genus *Polerovirus* is >10% amino acid sequence difference in any viral protein products as a new virus species threshold (Sõmera et al. 2021). Sequence analysis of this polerovirus showed that P0 and P1 shared <90% aa identity from any known poleroviruses, suggesting that the polerovirus isolate obtained in this study is a novel polerovirus. Combined with the yellowing and leaf crumple symptoms of gourd plants caused by this virus, we proposed the name bitter gourd yellowing crumple virus (BYCV) for this newly identified polerovirus.

The software ORF Finder was used to predict seven ORFs, namely, ORF0, ORF1, ORF1-2, ORF3a, ORF3, ORF4, ORF3-5, and three UTRs (Fig. 2) in the BYCV

genomic sequence, showing a typical genomic organization and structure of poleroviruses. The 717 nt ORF0 encodes a 27.3 kDa P0 protein, and the 68.4 kDa P1 protein is encoded by the 1881 nt ORF1. The ORF1-ORF2 consists of 3179 nt and encodes a P1-P2 fusion protein of 118 kDa through a -1 frameshift translation strategy with a featured slippery sequence 5'-GGGAAA C-3' (Tamm et al. 2009). Since ORF2 is translated by frameshift from ORF1 and thus shares an amino terminus with the product of ORF1. However, the ORF2 can not be translated to produce a separate protein. The ORF3a starts at ATA and ends at overlapping 20 nt with the 5'-terminal of ORF3. The 600 nt ORF3 and 576 nt ORF4 encode the P3 protein of 22.1 kDa and P4 protein of 21.2 kDa, respectively. In addition, the 572 nt of ORF3 overlapped with ORF4. As a readthrough protein (RTP) of 74 kDa, P3-P5 protein is translated from the ORF3-ORF5 frame. This read-through translation strategy means that ORF5 has no initiation codon for independent translation, but is translated via a readthrough of the termination codon at the end of ORF3. A 6-nt short sequence of ACAAAA, also processed in other poleroviruses, initiates at the 5'UTR of the viral genome (Knierim et al. 2013). This virus genome has an additional UTR of 82 nt between ORF2 and ORF3a and a 3'UTR of 165 nt.

### Comparative genome and phylogenetic analysis of the BYCV genome

Pairwise genome similarity of the 19 selected viral genomes of poleroviruses was compared using Sequence Demarcation Tool software v1.2 (SDT). BYCV is most closely related with CABYV (NC\_003688.1), sharing 79.80% nucleotide identity, based on the pairwise sequence identity of 18 viruses in the *Solemoviridae* family from the GenBank Database (Table 1). It is worth

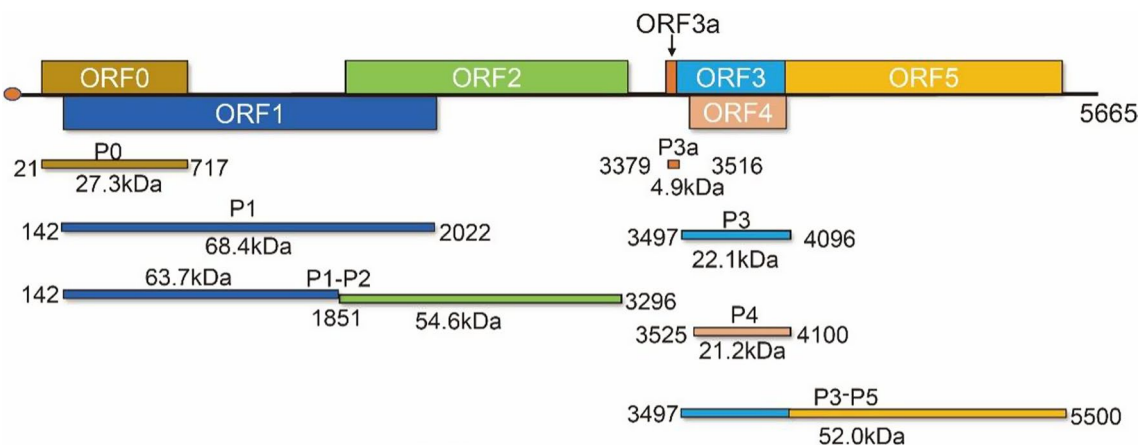


**Fig. 2** Schematic representation of the genome organization of bitter gourd yellowing crumple virus (BYCV). Open reading frames (ORFs) and deduced products of each RNA are indicated in colored boxes



**Table 1** Pairwise nucleotide and amino acid sequence identities of the open reading frames (ORFs) in the bitter melon yellowing crumple virus (BYCV) genome were calculated using the software Sequence Demarcation Tool v1.2

Genus	Virus abbreviation-GenBank number	Nucleotide identity (%) of complete genome	Nucleotide and amino acid identity (% nt/aa)						
			ORF0/P0	ORF1/P1	ORF1-ORF2/P1-P2	ORF3/P3	ORF3a/P3a	ORF4/P4	ORF3-ORF5/P3-P5
<i>Polerovirus</i>	CABYV-NC_003688.1	79.80	82.10/74.80	72.00/64.30	75.60/71.00	95.70/95.00	94.90/97.80	95.66/91.60	85.70/88.30
<i>Polerovirus</i>	PLRV-NC_001747.1	56.50	48.20/12.90	51.60/26.80	57.40/43.80	66.40/59.30	73.20/80.00	67.50/45.60	54.10/29.10
<i>Polerovirus</i>	BChV-NC_002766.1	58.00	45.30/10.70	51.30/26.10	56.70/44.40	69.30/64.80	82.50/64.40	68.40/46.20	59.20/43.20
<i>Polerovirus</i>	BMVYV-NC_003491.1	63.50	55.00/37.60	61.20/45.30	65.50/56.40	68.60/63.80	83.90/62.20	69.60/46.80	59.80/40.40
<i>Polerovirus</i>	CtRLV-NC_006265.1	55.30	46.30/10.00	51.90/29.50	57.00/46.60	60.70/49.20	67.20/70.50	58.70/33.90	53.60/28.40
<i>Polerovirus</i>	TVDV-NC_010732.1	57.20	51.00/23.20	55.00/27.40	60.70/48.10	63.40/54.00	71.00/77.80	62.90/10.90	52.00/23.30
<i>Polerovirus</i>	MABYV-NC_010809.1	72.601	78.40/69.30	72.60/65.80	74.80/73.40	80.20/76.90	73.90/71.10	80.70/66.30	67.90/56.90
<i>Polerovirus</i>	CLRDV-NC_014545.1	60.30	46.30/14.80	51.80/30.00	58.10/47.60	69.30/64.80	71.70/68.90	69.20/48.80	67.00/62.50
<i>Polerovirus</i>	PepVYV-NC_015050.1	62.401	49.80/12.00	54.40/22.90	60.60/48.10	65.90/50.80	73.20/80.00	65.30/12.20	64.90/50.60
<i>Polerovirus</i>	SABYV-NC_018571.2	60.601	46.70/13.40	49.70/21.20	56.10/39.30	80.30/78.40	71.00/95.46	80.80/67.90	67.90/56.50
<i>Polerovirus</i>	MYDV-RMV-NC_021484.1	56.40	43.80/11.60	51.10/28.20	57.30/45.70	67.10/57.80	51.40/42.20	68.30/37.70	56.80/35.20
<i>Polerovirus</i>	PABYV-NC_030225.1	62.80	48.60/13.50	54.10/16.60	57.90/35.40	86.70/84.40	73.90/77.80	87.20/77.50	73.20/59.70
<i>Polerovirus</i>	PuPV-NC_055513.1	60.50	49.40/12.60	48.40/14.90	54.00/35.40	86.80/84.40	72.50/77.80	87.30/77.00	72.90/66.50
<i>Polerovirus</i>	ScYLV-NC_000874.1	53.00	43.90/12.20	49.40/21.20	54.80/38.40	53.60/36.20	60.00/61.40	55.20/8.70	50.80/22.40
<i>Enamovirus</i>	PEMV-NC_003629.1	50.00	45.80/9.00	47.80/11.00	49.30/25.60	50.50/17.60	NA	NA	50.20/28.20
<i>Enamovirus</i>	CVEV-NC_021564.1	50.10	50.20/10.10	47.60/10.50	48.60/23.90	53.00/31.70	NA	NA	53.50/38.80
<i>Enamovirus</i>	GVEV1-NC_034836.1	48.10	48.70/10.10	44.20/9.10	48.30/23.30	46.20/28.00	NA	NA	45.60/24.80
<i>Polemovirus</i>	PnLV-NC_011543.1	50.70	42.50/8.40	49.10/18.10	NA	44.50/8.60	NA	NA	NA

noting that the highest a sequence similarity of P0, P1, P1-P2, and P3-P5 proteins of BYCV compared with other closely related viruses is 74.80%, 65.80%, 73.40%, and 88.30%, respectively. These results provide strong evidence that BYCV is a novel virus of the *Polerovirus* genus.

According to the above results, the genomic structure of BYCV had a high identity with the *Polerovirus* genus genomic structure. To show the classification of BYCV, a phylogenetic tree was constructed with a bootstrap of 1000 replications. Based on the mean of neighbor-joining phylogenetic analysis, phylogenetic trees were constructed using the nucleotide sequences

of the full-length genomes of BYCV and 18 viruses in the *Solemoviridae* family. All 19 viruses were separated into three clades, *Polerovirus*, *Enamovirus*, and *Polemovirus*. From the phylogenetic tree, BYCV had a closer relationship with CABYV-TW20 and was confidently located at the branch of the *Polerovirus* genus (Fig. 3). The phylogenetic trees constructed with amino acid sequences of the proteins P0, P1, P1-P2, and P3-P5 (encoded by ORF0, ORF1, ORF1-2, and ORF3-5, respectively) from the 19 viruses showed similar branches to that constructed with the full-length genome sequence (Additional file 2: Figure S1).

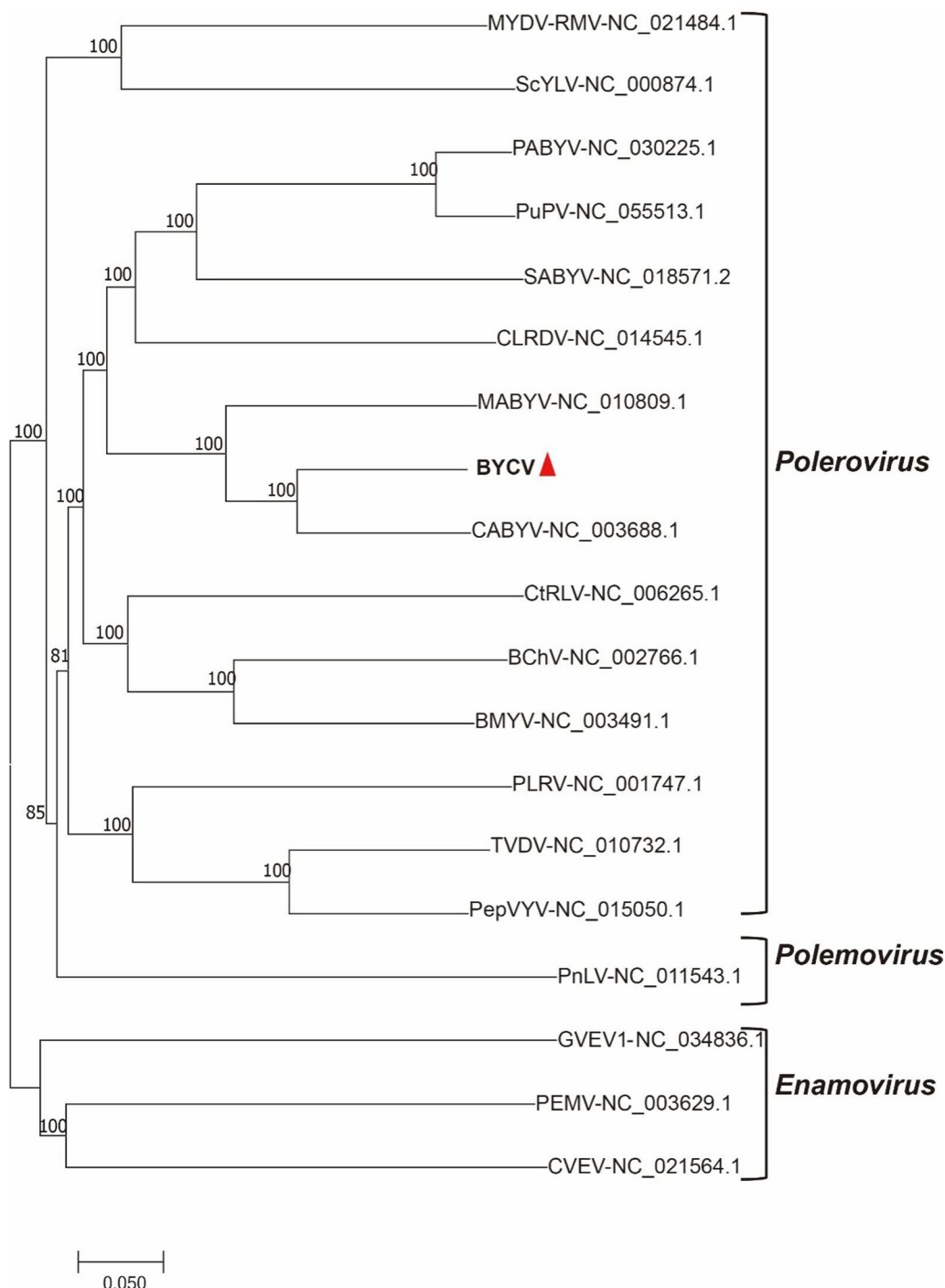


**Fig. 3** Phylogenetic analysis of BYCV and selected viruses of the family *Solemoviridae* based on the complete genome sequences. The accession numbers of selected solemovirids are shown as indicated. The phylogenetic tree was constructed using the neighbor-joining method implemented with MEGA 6, using bootstrap replicates of 1000

**Dynamic subcellular localization of BYCV-encoded viral proteins**

Dynamic subcellular localization of the proteins encoded by BYCV was further investigated to explore the

functions of the viral proteins. The seven BYCV-encoded viral proteins with yellow fluorescence protein (YFP) tags were transiently expressed in transgenic RFP-H2B *N. benthamiana* plants expressing RFP-H2B as a nuclear

indicator. Fluorescence signals from P0, P1, P1–P2, P3, P3a, P4, and P3–P5 fused YFP were observed at 24, 48, and 72 h post infiltration (hpi) by confocal microscopy (Figs. 4, 5 and Additional file 2: Figure S2). P0-YFP was mainly localized in the nucleoplasm and the nucleolus as previously reported for other P0 proteins (Wang et al. 2021), and the fluorescence of this protein mainly accumulated at 48 hpi and decreased at 72 hpi (Fig. 4a). Fluorescent signals of P1-YFP were primarily present in the nucleoplasm, the nucleolus, and the perinuclear

regions. Using an endoplasmic reticulum (ER) marker mCherry-HDEL, we found that P1-YFP co-localized with mCherry-HDEL at ER in *N. benthamiana* leaves at 36 hpi (Additional file 2: Figure S4a). The fluorescence of P1-YFP aggregates became brighter at 48 hpi, subsequently darkened at 72 hpi (Fig. 4b). P1-P2-YFP was also observed in the nucleoplasm and nucleolus that is similar to P0-YFP, but the difference is that the yellow fluorescent signals on cytomembrane at 24 hpi and those at 48 and 72 hpi accumulated in the perinuclear regions (Fig. 4c). P3a-YFP was

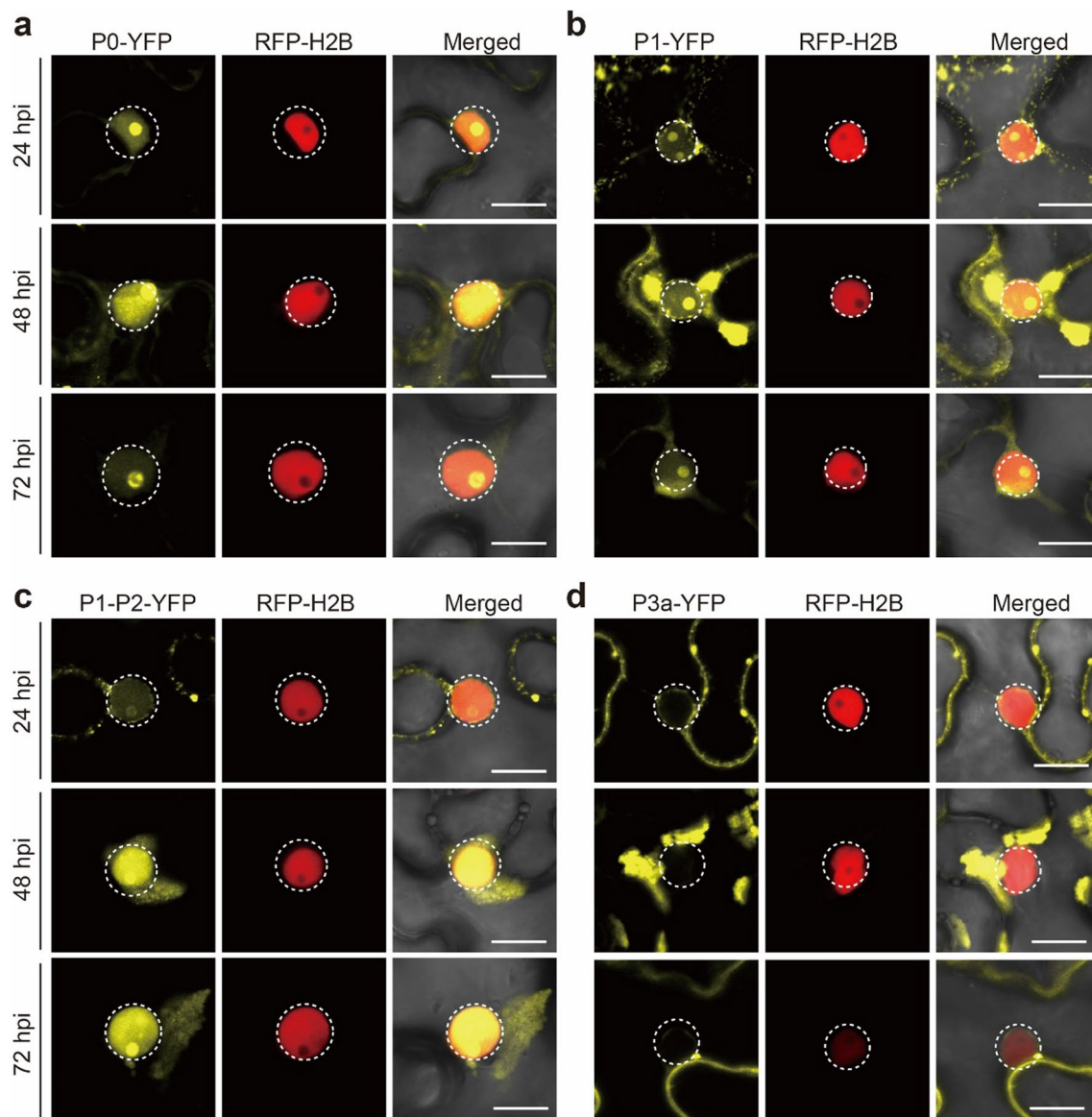


**Fig. 4** Confocal images of BYCV P0, P1, P1-2, or P3a proteins fused with YFP. RFP-H2B transgenic *Nicotiana benthamiana* leaves were infiltrated with *Agrobacterium* cultures to express P0-YFP (a), P1-YFP (b), P1-2-YFP (c), or P3a-YFP (d). Confocal images were taken 24, 48, and 72 h post infiltration (hpi). The YFP signal is shown in yellow. The nuclei of tobacco leaf epidermal cells are marked by RFP-H2B (red). This experiment was repeated three times independently, and more than 20 cells per sample were observed each time; representative results are shown; scale bars: 10  $\mu$ m

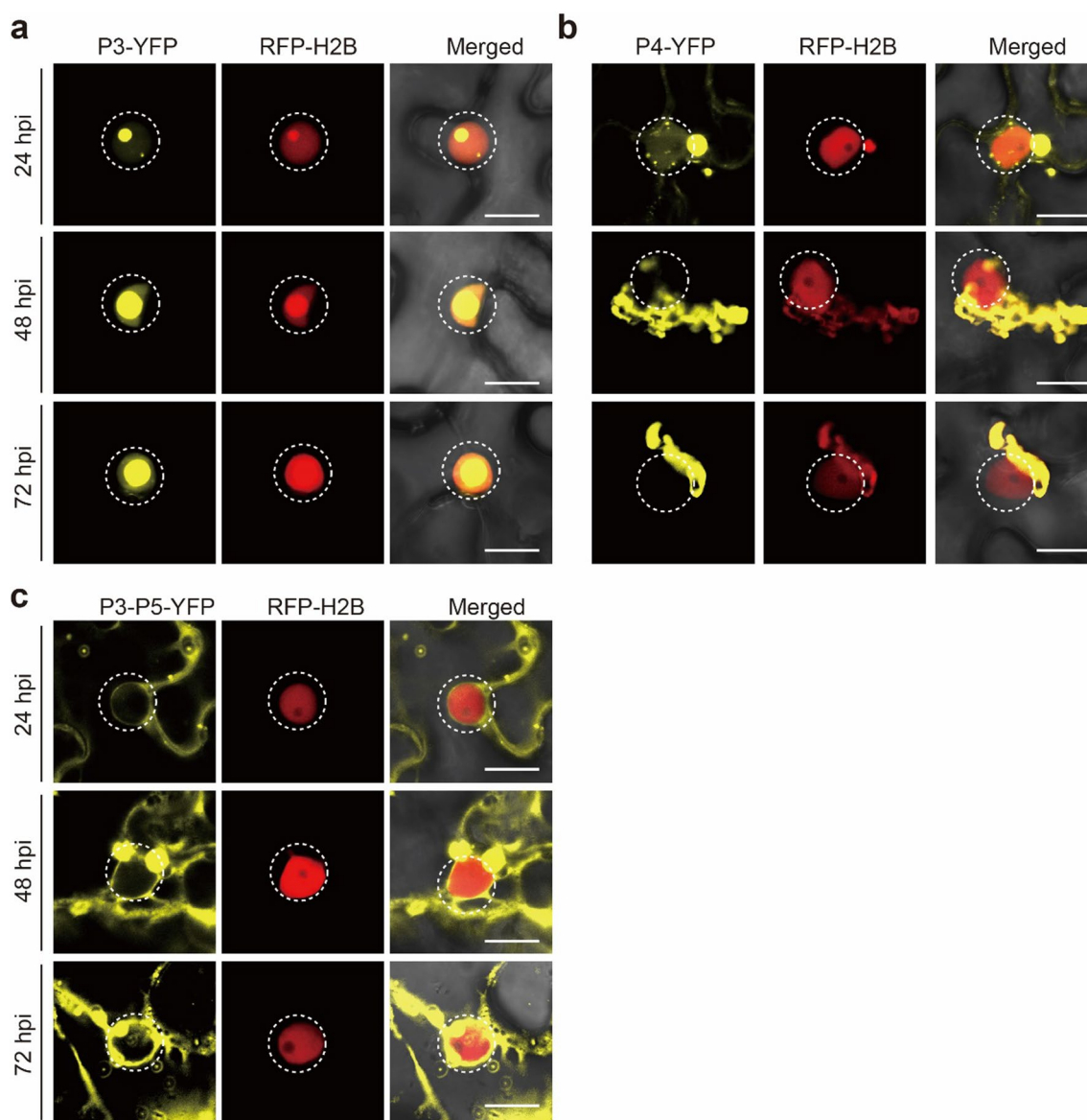


**Fig. 5** Confocal images of BYCV P3, P4, or P3-5 proteins fused with YFP. RFP-H2B transgenic *N. benthamiana* leaves were infiltrated with *Agrobacterium* cultures to express P3-YFP (**a**), P4-YFP (**b**), or P3-5-YFP (**c**). Confocal images were taken at 24, 48, and 72 hpi. The nuclei of tobacco leaf epidermal cells are marked by RFP-H2B (red). This experiment was repeated three times independently, and more than 20 cells per sample were observed each time; representative results are shown; scale bars: 10  $\mu$ m

distributed in the cell membrane, perinuclear regions, and plasmodesmata (PD) (Fig. 4d). To verify the PD localization, P3a-YFP, a PD marker TMV MP-mRFP, was used to co-express with P3a-YFP in *N. benthamiana* leaves. At 36 hpi, the co-localization of P3a-YFP with PD labelled by TMV MP-mRFP was observed under confocal microscope (Additional file 2: Figure S4c) (Gong et al. 2022). Therefore, consistent with the previous finding, the P3a protein localized at PD is required for viral intercellular movement (Smirnova et al. 2015). The fluorescent signals

of P3a-YFP at 48 hpi and 72 hpi were more robust than those at 24 hpi (Fig. 4d). It is worthy of note that P3-YFP was localized in the nucleoplasm and the nucleolus but displayed a different subcellular localization with P0-YFP. At 48 and 72 hpi, the P3-YFP fluorescent signal disappeared in the nucleoplasm and became much brighter in the nucleolus only (Fig. 5a). P4-YFP formed small granules in the nucleus and the cytoplasm at 24 hpi. While P4-YFP displayed a colocalization with RFP-H2B in the perinuclear regions after 48 hpi, which could guide the



nuclear export of RFP-H2B, and formed protein aggregates (Fig. 5b). According to a previous report, the transport of viral genomes required MP moving through ER and PD (Schoelz et al. 2011). The P4 protein of other polioviruses was also reported as a movement protein (Li et al. 2020). In order to further verify the localization of P4, P4-YFP with the ER marker mCherry-HDEL and the PD marker TMV MP-mRFP were transiently expressed in *N. benthamiana* leaves, respectively. As shown in Additional file 2: Figure S4b, d, the localizations of P4 at ER and PD were observed. Unlike the protein localization described above, P3-P5-YFP formed some small granules in the cytoplasm. The fluorescence of these granules formed protein aggregates and became brighter at 48 and 72 hpi (Fig. 5c). In addition, BYCV-encoded proteins with an N-terminal YFP were also expressed in transgenic RFP-H2B *N. benthamiana* plants.

Fused proteins displayed similar subcellular localizations when fused with an N-terminal YFP or a C-terminal YFP by comparing Figs. 4, 5 and Additional file 2: Figure S3 under confocal microscope. However, except for the P1 protein, fluorescent signals from P1 proteins with an N-terminal YFP gathered around the nucleus rather than at ER.

To observe the dynamic changes in the accumulation of the BYCV-encoded proteins, total proteins were extracted from P0-YFP, P1-YFP, P1-P2-YFP, P3a-YFP, P3a-YFP, P4-YFP, or P3-P5-YFP -expressing leaves at 24, 48, and 72 hpi. Protein levels from 24 to 72 hpi were shown in Fig. 6. The accumulation of all BYCV-encoded proteins-YFP at 24 hpi was less than at 48 hpi. P0-YFP, P1-YFP, and P3-P5-YFP had the most protein accumulation at 48 hpi, while P1-P2-YFP, P3a-YFP, and P3-YFP had the most protein accumulation at 72 hpi. The

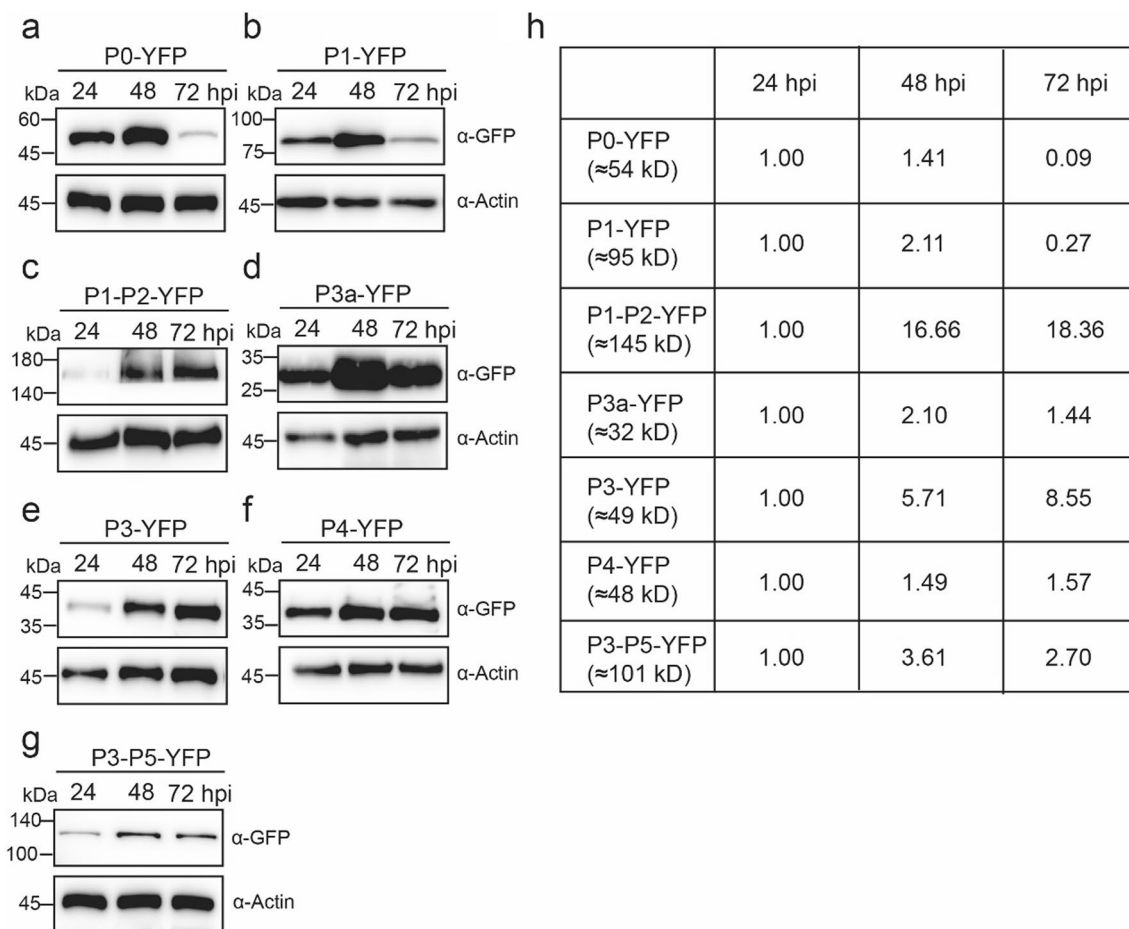


**Fig. 6** Dynamic protein accumulation of BYCV-encoded viral proteins. *Agrobacterium* cultures expressing P0-YFP, P1-YFP, P1-P2-YFP, P3a-YFP, P3-YFP, P4-YFP, or P3-P5-YFP adjusted to an optical density at 600 nm ( $OD_{600}$ ) = 0.7 was infiltrated in *N. benthamiana* leaves. Total proteins were extracted from P0-YFP, P1-YFP, P1-P2-YFP, P3a-YFP, P3-YFP, P4-YFP, or P3-P5-YFP infiltrated leaves at 24, 48 and 72 hpi. An anti-GFP was used to detect antibody accumulation of protein P0-YFP (a), P1-YFP (b), P1-P2-YFP (c), P3a-YFP (d), P3-YFP (e), P4-YFP (f), or P3-P5-YFP (g) at 48, 72, and 96 hpi. A specific anti-Actin antibody was used as a loading in western blotting assays. h The protein accumulation from western blotting images was digitized by Image J, and the data at 24 hpi was set to 1

accumulation of P4-YFP displayed no apparent change after 48 hpi. To better observe the protein changes over time, the protein accumulation was digitized by Image J, and the data at 48 and 72 hpi were normalized to that at 24 hpi (set to 1). These data were consistent with the results observed by confocal microscopy. The conclusion of reverse transcription-quantitative real-time PCR (RT-qPCR) analysis showed that the decrease in seven viral protein accumulations was mainly due to the decrease in the viral RNA transcript accumulation from 48 to 72 hpi (Additional file 2: Figure S5).

### **P0 is a virulence determinant that leads to severe symptoms in *N. benthamiana* plants**

The P0 protein is an important pathogenic factor in many reported poleroviruses (Wang et al. 2023). To assess the biological relevance of the BYCV-encoded P0 protein in virus infection, we constructed a potato virus X (PVX) vector-based recombinant carrying the P0 gene (PVX-P0) for ectopic overexpression of this viral ORF. *A. tumefaciens* cultures carrying the empty binary vector (Mock), PVX, PVX-P0, or PVX-HC-Pro (HC-Pro cistron of turnip mosaic virus) were agroinfiltrated to 5–6 leaves-old *N. benthamiana* plants. The inoculated plants were maintained to observe viral symptom appearance and analyze viral protein accumulation in the newly emerged leaves. At 10 dpi, the symptoms of PVX-inoculated control plants displayed obvious mosaic symptoms (Fig. 7a). However, the PVX-P0 infected plants developed more severe mosaic, chlorosis, leaf curling, and necrotic symptoms at 10 dpi. All 30 tested plants agroinoculated with PVX-P0 showed the symptoms mentioned above in systemically infected leaves at 20 dpi (Fig. 7a). Of note, PVX-infected plants first exhibited mosaic symptoms from 5 to 14 dpi, followed by a predominance of light chlorotic spots as symptom recovered at 20 dpi (Fig. 7a). The positive control, PVX-HC-Pro-infected plants, exhibited the typical HC-Pro-associated leaf curling and necrosis phenotype, in addition to the PVX-caused mosaic symptom at 10 and 20 dpi (Fig. 7a). To further confirm the effect of P0 on the accumulation of PVX in infected plants, we analyzed the accumulation of the PVX coat protein (CP) from the above-inoculated plants using anti-PVX-CP antibodies by western blotting at 10 and 20 dpi. The result showed that more PVX CP protein accumulated in PVX-P0 infected plants compared with PVX infected plants at 20 dpi, indicating that BYCV P0 is a virulence factor that promotes PVX infection in *N. benthamiana* plants (Fig. 7b).

Meanwhile, we observed that newly emerged leaves of PVX-P0-infected plants showed significant necrosis and wrinkling after 15 dpi (Fig. 7c, left panels), whereas PVX-infected leaves did not. To determine the cause

of necrosis after PVX-P0 infection, the production of ROS (accumulation of H<sub>2</sub>O<sub>2</sub>) was analyzed using the 3,3'-diaminobenzidine (DAB) uptake method. In the presence of H<sub>2</sub>O<sub>2</sub>, DAB aggregation produced dark brown precipitates on the leaves (Thordal-Christensen et al. 1997). We found that high concentrations of H<sub>2</sub>O<sub>2</sub> accumulated in PVX-P0 systemically infected leaves (Fig. 7c, PVX-P0).

### **P0 blocks local and systemic RNA silencing triggered by GFP RNA**

RNA silencing is one of the most potent antiviral immunity in plants (Baulcombe 2022). To establish a successful infection, almost all viruses encode at least one RSS to counterattack RNA silencing (Kon et al. 2007; Li et al. 2014; 2018a; 2018b; Li and Wang. 2019). Previous reports have shown that the P0 protein from several poleroviruses is an RSS (Cai et al. 2023). To identify whether the BYCV P0 is an RSS, we agroinfiltrated the GFP-transgenic *N. benthamiana* 16c plants with mixed *A. tumefaciens* cultures carrying 35S-GFP with empty vector (Vec), P0, or P19 in a ratio of 1:1. At 4 dpi, we observed that GFP fluorescence intensity decreased substantially in the 35S-GFP with Vec co-infiltrated leaf patches. At the same time, it was enhanced in the 35S: GFP with P0 or with P19 (a well-studied RSS of tomato bushy stunt virus, used as a positive control) co-infiltrated leaf patches under UV light (Fig. 8a). qRT-PCR and western blotting analyses showed that the co-expression of P0 or P19 resulted in more GFP RNA and higher protein accumulations, although the effect of P0 appeared to be weaker than that of P19 (Fig. 8b, c).

Furthermore, the PVX vector was also used to express P0 to analyze its RNA silencing suppression activity. *A. tumefaciens* cultures harboring 35S-GFP and negative control (PVX), PVX-P0, or PVX-HC-Pro (a positive control), respectively, were co-infiltrated into 16c *N. benthamiana* leaves. Consistent with our previous results, the expression of P0 from a PVX vector could also efficiently suppress GFP-induced local RNA silencing at 7 dpi (Fig. 8d–f). The agroinfiltrated plants were maintained to examine systemic silencing in the newly emerged leaves at 15 dpi. In the negative controls, the upper young leaves of 75% of infiltrated plants turned red under UV light, indicating systemic RNA silencing (Fig. 8g); however, the newly emerged leaves in more than 90% of plants co-infiltrated with P0 and HC-Pro remained green under UV light (Fig. 8g), suggesting that both P0 and HC-Pro can suppress the ssGFP-induced systemic RNA silencing. These findings provide persuasive evidence that P0 can suppress GFP-induced RNA silencing similar to other P0 proteins of poleroviruses but showed weak RNA silencing suppression activity.

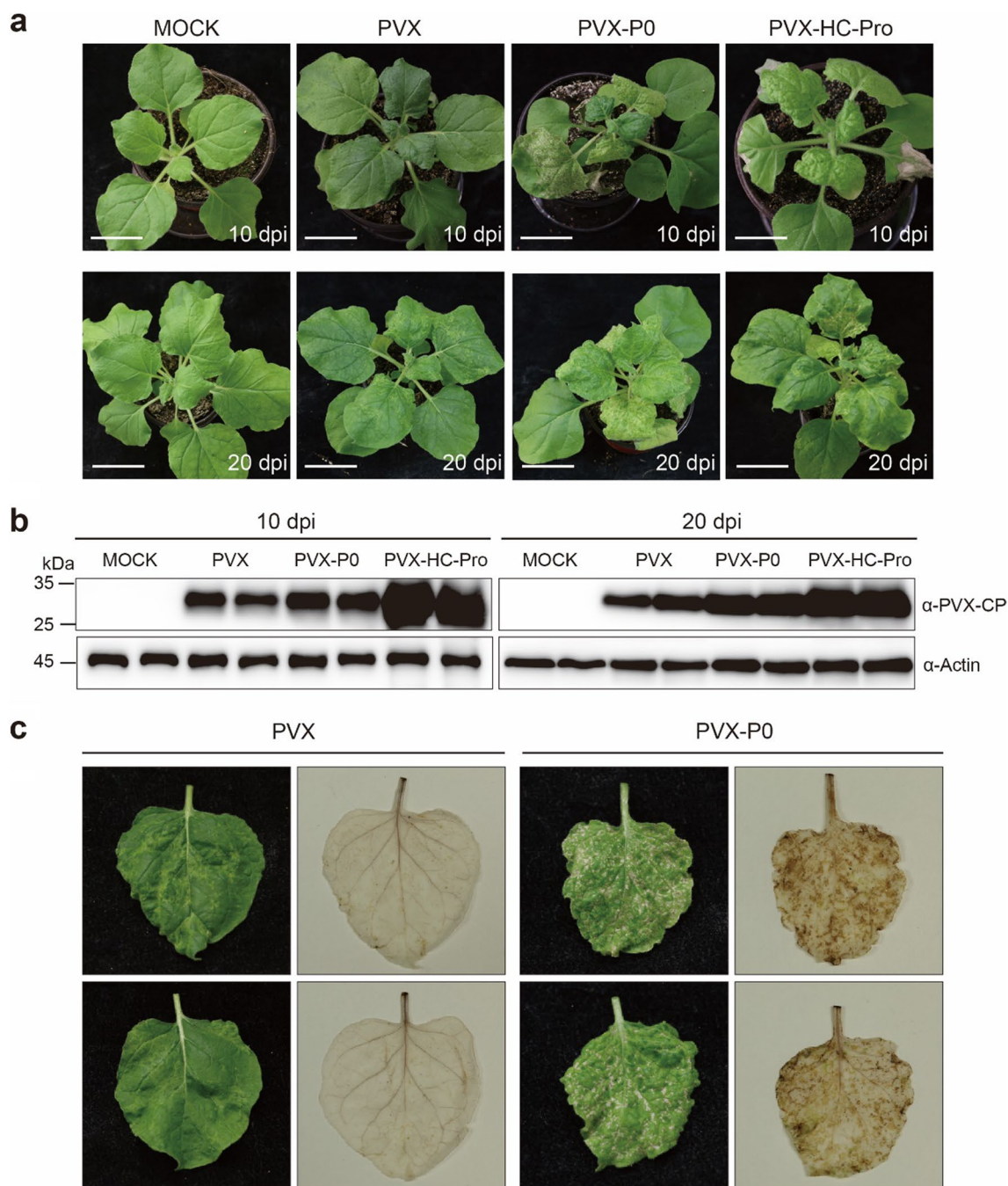


**Fig. 7** Symptoms exhibited by *N. benthamiana* plants following inoculation with PVX, PVX-P0, or PVX-HC-Pro. **a** Viral symptoms were elicited on *N. benthamiana* plants by inoculating Mock (infiltration buffer), PVX, PVX-P0, or PVX-HC-Pro (positive control) at 10 and 20 dpi. Bars = 4 cm. **b** western blotting analyses of PVX CP accumulation with specific anti-PVX-CP antibodies in systemic leaves from **(a)**. Western blotting analyses of loading control with specific anti-Actin antibodies in systemic leaves from **(a)**. This experiment was repeated three times with similar results. **c** The symptoms and DAB staining of systemic leaves from *N. benthamiana* plants infected by PVX and PVX-P0 at 20 dpi



## Discussion

Since abundant small RNAs derived from viral RNA were generated in virus-infected cells, sRNAs-based deep sequencing technology and bioinformatics have become highly efficient and reliable approaches for identifying novel virus species in eukaryotes. This study identified and characterized a distinct member of the *Polerovirus* genus (family *Solemoviridae*) from bitter melon plants. Sequence analysis of the polerovirus identified in this study showed that the amino acid sequences of P0 and P1 shared <90% aa identity from the other known poleroviruses, which fits ICTV demarcation criteria for the *Polerovirus* genus as a distinct virus species. With the yellowing and leaf crumple symptoms of melon plants caused by this virus, bitter melon yellowing crumple virus (BYCV) is proposed for this novel viral species.

The BYCV identified in this study shares a typical genome feature and structure with known poleroviruses. Phylogenetic analysis of the complete genome sequence of BYCV with other previously reported species of the family *Solemoviridae* also revealed that BYCV was grouped into poleroviruses but separated from members of the genera *Enamovirus*, *Polemavirus*, and *Sobemovirus*. A detailed BLASTn and phylogenetic analysis showed that this virus was closely related to CABYV, a polerovirus that has been described to cause severe damage to the crops of Cucurbitaceae. In the phylogenetic tree of full-length genome sequences, BYCV and CABYV cluster in one branch, and this branch is independent of other branches. The P0 and P3–P5 proteins of both viruses also cluster in the same branch, suggesting that they are genetically close (Fig. 3 and Additional file 2: Figure S1). CABYV is a member of the genus *Polerovirus* in the family of *Solemoviridae*. Like other poleroviruses, CABYV is limited to phloem tissues in infected plants.

The subcellular localization of some poleroviral proteins has been analyzed in a targeted manner. This study investigated the subcellular localization of all

BYCV-encoded proteins and the accumulation of each protein. P0, as an extensively studied viral protein, is mainly localized in the nucleus, particularly in the nucleolus (Wang et al. 2021). Consistent with this finding, P0 of BYCV was also localized predominantly in the nucleolus (Fig. 4a). The protein accumulation of P0-YFP was decreased at 72 hpi, probably related to its function as a weak RSS and a pathogenicity factor (Figs. 4a, 6a, and 8). The fluorescence of P1-YFP localized in the nucleolus and the perinuclear regions and was the brightest at 48 hpi. We also found that the protein and RNA levels of P1-YFP were the lowest at 72 hpi, suggesting that the expression of P1-YFP is affected by RNA and protein-mediated degradation (Figs. 4b, 6b and Additional file 2: Figure S5). The location of P1-P2-YFP changed over time with increasing fluorescence intensity and protein accumulation after 24 hpi, slowly decreasing RNA level after 48 hpi, indicating that P1–P2 does not follow host RNA and protein-mediated degradation mechanisms (Figs. 4c and 6c, Additional file 2: Figure S5). P3a-YFP located in the cell membrane and in perinuclear space, which the protein accumulation and RNA accumulation at 48 hpi similar to that of P1-YFP, suggesting that the expression of P3a-YFP is susceptible to both RNA and protein-mediated degradation (Figs. 4d, 6d and Additional file 2: Figure S5). P3-YFP was localized in the nucleoplasm and the nucleolus, contributing to the increase in the nucleoplasm area. We found no apparent change in P3 protein accumulation and RNA level after 48 hpi (Figs. 5a, 6e and Additional file 2: Figure S5). P4-YFP could guide the nuclear export of RFP-H2B and form protein aggregates. Protein accumulation of P4 also showed no significant change after 48 hpi. However, the RNA level decreased, suggesting that the expression of P4-YFP is unaffected by RNA- and protein-mediated degradation (Figs. 5b, 6f). The results of fluorescence, protein accumulation, and RNA level indicated that the expression

(See figure on next page.)

**Fig. 8** P0 suppresses GFP-induced RNA silencing. **a** 16c *N. benthamiana* plants co-infiltrated with *A. tumefaciens* cultures expressing GFP (35S-GFP) and vector control (Vec), BYCV P0 (P0), or TBSV 19 (P19, a positive control) were photographed under UV light at 4 dpi. Bars = 2 cm. **b** qRT-PCR analysis of relative GFP expression levels in the agroinfiltrated leaf patches from **a**. Three plants were analyzed for each treatment; this experiment was repeated three times with similar results. Error bars represent  $\pm$  SD ( $n=3$ ), and *NbActin2* was used as an internal reference. **c** western blotting analyses of the GFP protein accumulation in the agroinfiltrated leaf patches as indicated in **(a)**. **d** The 16c *N. benthamiana* plants co-infiltrated 35S-GFP and PVX, or PVX-P0, or PVX-HC-Pro, were photographed under UV light at 7 dpi. Bars = 2 cm. **e** qRT-PCR analysis of relative GFP expression levels in the agroinfiltrated leaf patches from **(d)**. Error bars represent  $\pm$  SD ( $n=3$ ), and *NbActin2* was used as an internal reference. Student's *t*-test was used to analyze each data group statistically, and double asterisks indicate significant statistical differences (\*\* $P < 0.01$ ) between the two treatments. **f** western blotting analyses of GFP and PVX CP accumulation in the agroinfiltrated leaf patches as indicated from **(d)**. **g** The 16c *N. benthamiana* plants co-infiltrated 35S-GFP and PVX, or PVX- or PVX-HC-Pro, were photographed under UV and white light at 20 dpi. Bars = 4 cm. **h** qRT-PCR analysis of relative GFP expression levels in systemic leaves from **(g)**. Error bars represent  $\pm$  SD ( $n=3$ ), and *NbActin2* was used as an internal reference. Student's *t*-test was used to analyze each data group statistically, and double asterisks indicate significant statistical differences (\*\* $P < 0.01$ ) between the two treatments. **i** western blotting analyses of GFP and PVX CP accumulation in systemic leaves from **(g)**. Western blotting analyses of the Actin accumulation with a specific anti-Actin antibody served as a loading control **(c)**, **(f)**, and **(i)**. At least 6 plants were used in each independent systemic experiment. The agroinfiltration experiment, qRT-PCR and Western blotting analyses were repeated three times with similar results in this figure



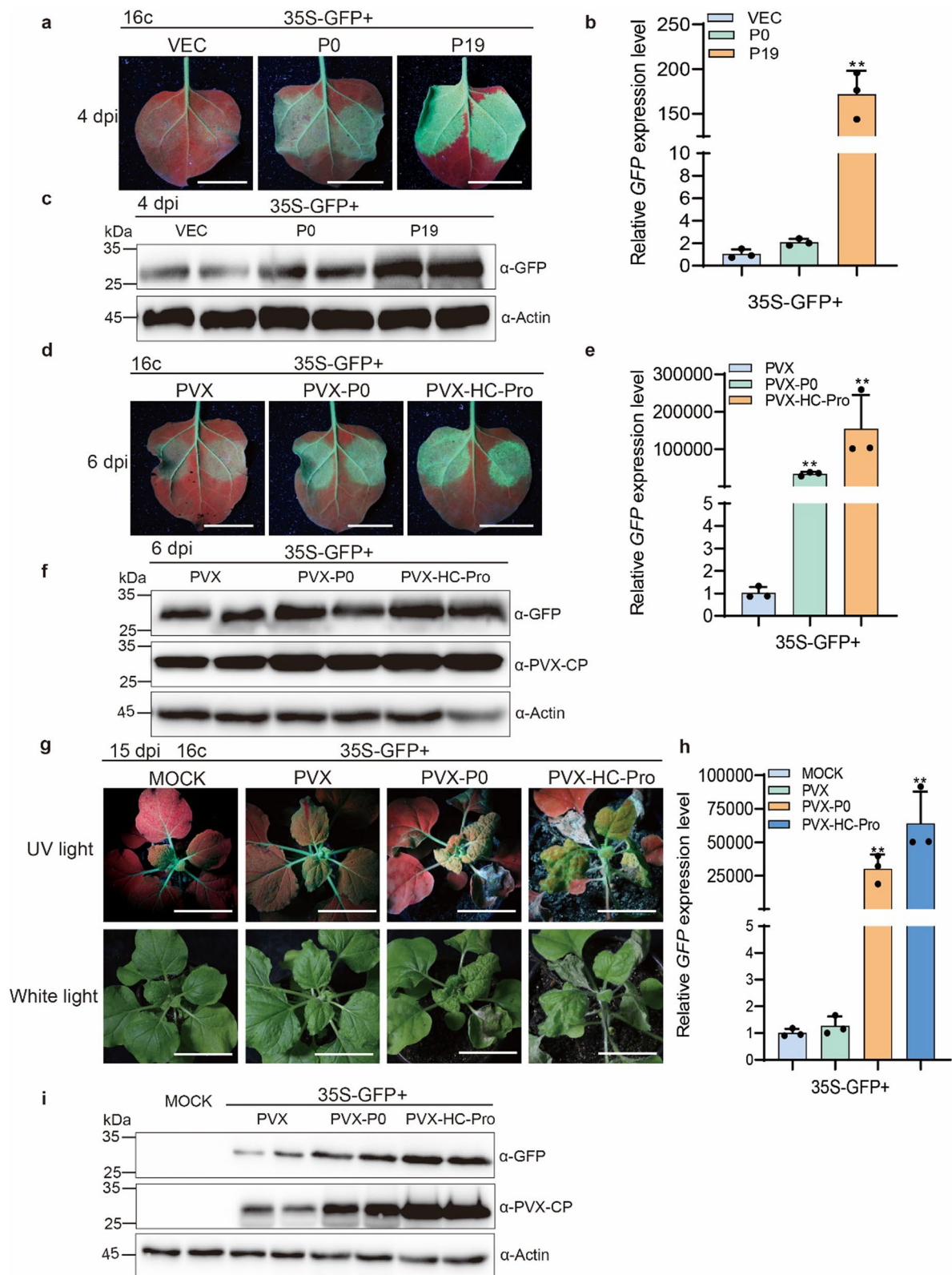


**Fig. 8** (See legend on previous page.)

of P3-P5-YFP is susceptible to both RNA- and protein-mediated degradation (Figs. 6c, 7g and Additional file 2: Figure S5).

During the long co-evolution of plants and viruses, plants have evolved many layers of defense responses against viral infections, including DNA methylation, RNAi-based antiviral immunity, autophagy, N-gene-mediated resistance, etc. (Yang and Li 2018; Guo et al. 2019; Yang et al. 2020; Li et al. 2022b; Yang and Liu 2022; Chen et al. 2023). Among these, RNAi is the most conserved immunity that can restrict plant virus invasions. However, to counter-attack these defenses and adapt to host plants, almost all known plant viruses encode at least one RSS to inhibit RNA silencing (Guo et al. 2019; Li and Wang 2019). Many research teams have extensively explored the mechanisms underlying host antiviral immunity and the RSS-mediated viral counter-defense (Li and Wang 2019; Baulcombe 2022). The P0 protein of poleroviruses, as a strong RSS, emerged first in the beet western yellows virus. The interaction existed between the F-box motif of P0 protein and homologs of S-phase kinase-related protein 1 (SKP1) as a core subunit of the multicomponent SCF family of ubiquitin E3 ligases. This interaction was disrupted by a mutant of the F-box motif, leading to a weaker viral pathogenicity (Pazhouhandeh et al. 2006). The ectopic expression of P0 triggered the degradation of AGO1 and caused developmental abnormalities in transgenic *A. thaliana* (Bortolamiol et al. 2007; Chiu et al. 2010). The mechanism of this degradation does not follow ubiquitin or proteasomes (Baumberger et al. 2007). Here, using the PVX vector, we also found that the BYCV P0 protein is an important pathogenicity factor which induced obvious viral symptoms in *N. benthamiana* plants and could repress RNA silencing (Figs. 7, 8), indicating that the P0 protein is evolutionarily conserved among different poleroviruses.

## Conclusions

In this study, we identified a novel virus of the *Polerovirus* genus infecting bitter melon plants and named it bitter melon yellowing crumple virus (BYCV). We investigated the dynamic subcellular localization and accumulation of BYCV-encoded viral proteins. One of the notable results of this study is that the P0 protein of BYCV is a virulence determinant and RNA silencing suppressor, which might play a vital role in viral pathogenicity.

## Methods

### Sample collection, total RNA extraction, and qRT-PCR

Bitter melon plants showing yellowing and crumple symptoms were collected from Hainan Province of China in 2021. Plant materials containing symptoms were used for RNA extraction and small RNA sequencing. RNA

extraction was performed as previously described with minor modifications (Ge et al. 2023). Total RNA was isolated from 0.1 g of each fresh plant sample using the TRIzol extracting solution (Invitrogen, Carlsbad, CA, USA) according to the manufacturer's instructions.

The PrimeScript™ reagent kit with gDNA eraser (TaKaRa, Japan) retrotranscribed RNA to form cDNA following the manufacturer's protocol. The qRT-PCR was performed using a Roche Light Cycler 96 system (Roche Applied Primer NbActin as a comparable standard, and the relative expression level of the target protein was analyzed following the calculations method of  $2^{-\Delta\Delta CT}$ . All primers used in the qRT-PCR experiments are shown in Additional file 1: Table S1.

### Small RNA library construction, sequencing, and data processing

A small RNA sequencing library was constructed using the TruSeq™ Small RNA Sample Prep Kits (Illumina, San Diego, USA). The constructed library was sequenced by Illumina HiSeq 2000/2500 platform (Lianchuan, Beijing, China). The raw data were pre-processed with ACGT101-miR (LCSciences, Houston, Texas, USA) developed by Lianchuan Biologics. Clean reads were produced by processing raw reads: cutting adaptor, scanning length, and removing junk reads and host genome. Sequence assembled was performed with the Velvet program to obtain longer contigs. BLASTN of the NCBI GenBank database was used to compare assembled contigs to analyze the identity of the candidate virus.

### The strategy of whole genome amplification

The full-length viral genome was separated into six fragments to amplify. Based on the assembled contigs of the sRNAs sequencing data, six pairs of primers with overlapping regions between two adjacent sequences (BYCV-1F/1R, BYCV-2F/2R, BYCV-3F/3R, BYCV-4F/4R, BYCV-5F/5R, and BYCV-6F/R Additional file 1: Table S1) were designed to obtain the completed sequence of the viral genome. Viral cDNA, as the template of PCR amplification, six fragments of the full-length sequence were amplified by KOD high-fidelity enzyme (Takara, Beijing, China) and cloned into a pEASY-Blunt vector for sequencing. Based on known candidate sequences, the viral genome's 5' and 3' terminal sequences were amplified by KOD and obtained by DNA sequencing.

### Virus genome sequence analysis and phylogenetic analyses

Viral genome encoded ORF were predicted using ORF Finder and corrected by referring to the GenBank database (Chen et al. 2022). The pairwise sequences were compared using the Sequence Demarcation Tool (SDT)

v1.2 (Muhizi et al. 2014). Phylogenetic trees were constructed with MEGA software version 7 using neighbor-joining with 1000 bootstrap replicates after aligning sequences with the software Muscle (Li et al. 2022a).

### Plasmids and constructs

The completed sequence of BYCV was constructed into a pEASY-Blunt vector named T-BYCV. In this study, all vectors used for subcellular localization experiments and viral RNA silencing suppression assay experiments were constructed by gateway technology. The sequences of the BYCV-encoded proteins, including P0, P1, P1–P2, P3, P4, and P3–P5, were amplified by PCR. The KOD high-fidelity enzyme (Takara, Beijing, China) and the T-BYCV plasmid as a template were used to generate viral protein PCR products. The P0, P1, P1–P2, P3, P4, and P3–P5 ORF were fused to transient expression vectors pEarleygate101 (with C-terminal YFP) and pEarleygate104 (with N-terminal YFP) for analyzing their subcellular localization. The PBA-Flag-4xMyc recombinant construct with P0 was used in the RNA silencing suppression assay experiment. The P0 protein sequence was amplified from T-BYCV using primer pairs: PVX (Cla I)-BYCV-P0-F and PVX (Sal I)-BYCV-P0-R to construct the recombinant PVX expression vector. The PCR product and PVX vector were digested with *Cla* I and *Sal* I to generate PVX-P0, which was transformed into *A. tumefaciens* strain GV3101. All primers used in this study can be found in Additional file 1: Table S1.

### Confocal microscopy

The fluorescence of subcellular localization of viral proteins with YFP marker was observed and photographed under confocal microscopy (Carl Zeiss LSM T-PMT, Germany) at 24, 48 and 72 hpi. YFP was excited at 514 nm, and the emitted light was captured at 565–585 nm (Zhang et al. 2023). 552 nm excitation and 590 nm emission filters were used to capture RFP fluorescence. The ZEN 2 (Carl Zeiss Microscope GmbH2011) software was used to analyze the collected images.

### Protein extraction and Western blotting

The total protein of plant leaves was extracted using a protein extraction buffer (50 mmol/L Tris–HCl pH 6.8, 4.5% SDS, 7.5% 2-mercaptoethanol, 9 M carbamide). Total proteins were separated by electrophoresis in 12% sodium dodecyl sulfate–polyacrylamide gel electrophoresis (SDS-PAGE) and were transferred to a nitrocellulose (NC) membrane with constant voltage. Primary mouse polyclonal antibodies were used for the target protein of detection by immunoblotting. In this study, primary antibodies were used as follows: anti-GFP (1:5000; ROCHE, USA) and anti-PVX CP (1:5000) (Wu

and Zhou 2015; Wu et al. 2012). Anti-mouse IgG HRP as a secondary antibody combined with peroxidase. A high-signal ECL western blotting substrate (Tanon, Shanghai, China) was used to detect the target protein following a Tanon chemiluminescence detection system. A specific antibody was used as a loading control in Western blotting analyses.

### Assay of PTGS suppression function of P0 protein encoded by BYCV

According to the previous report, 35S-P19 (TBSV 19) and 35S-GFP (the *Agrobacterium* expressing GFP) are cited for detecting the function of the RNA-silencing suppressor from viral protein P0 (Li et al. 2015). A mixture of the *agrobacterium* cultures expressing 35S-GFP and P0 was infiltrated into transgenic 16c *N. benthamiana*, which expresses green fluorescent protein (GFP, line 16c). A mixture of the *Agrobacterium* of 35S-GFP and 35S-P19 is used for positive control. Flag-Gus and 35S-GFP *Agrobacterium* mixture is used for negative control. After 4 dpi, UV light was used to observe for infiltration of the leaves. PVX, PVX-P0, and PVX-HC-Pro were mixed with 35S-GFP, respectively, and infiltrated into transgenic 16c *N. benthamiana*. UV and white light were used to observe infiltrated transgenic 16c *N. benthamiana* in 6 and 15 dpi.

### Abbreviations

BYCV	Bitter gourd yellowing crumple virus
CABYV	Cucurbit aphid-borne yellows virus
CP	Coat protein
dpi	Days post infiltration
hpi	Hours post infiltration
MP	Movement protein
Nb	<i>Nicotiana benthamiana</i>
NC	Nitrocellulose
ORFs	Open reading frames
PVX	Potato virus X
qRT-PCR	Quantitative real-time reverse transcription PCR
RdRP	RNA-dependent RNA Polymerase
RTP	Readthrough protein
SABYV	Suakwa aphid-borne yellows virus
SDS-PAGE	Sodium dodecyl sulfate–polyacrylamide gel electrophoresis
sRNAs	Small RNAs
siRNAs	Small interference RNAs
SDT	Sequence Demarcation Tool
SKP1	S-phase kinase-related protein 1
UTRs	Untranslated regions
RSS	RNA-silencing suppressor
YFP	Yellow fluorescence protein

### Supplementary Information

The online version contains supplementary material available at <https://doi.org/10.1186/s42483-023-00192-y>.

**Additional file 1: Table S1.** Primers were used in all experiments in this study.

**Additional file 2: Figure S1.** Phylogenetic analysis of bitter gourd yellowing crumple virus (BYCV) encoded protein. **Figure S2.** A full view of

subcellular localizations of the BYCV encoded proteins-YFP (a) or YFP-BYCV encoded proteins (b) transiently expressed in RFP-H2B transgenic *Nicotiana benthamiana* leaves at 36 hpi. **Figure S3.** Confocal images of the BYCV encoded P0, P1, P1-2, P3a, P3, P4, or P3-5 proteins fused with an N-terminal YFP. RFP-H2B transgenic *Nicotiana benthamiana* leaves were infiltrated with *Agrobacterium* cultures to express YFP-P0, YFP-P1, YFP-P1-2, YFP-P3a, YFP-P3, YFP-P4, or YFP-P3-5. **Figure S4.** P1 and P4 co-localized with an endoplasmic reticulum (ER) marker: mCherry-HDEL, and P3a and P4 co-localized with a plasmodesmata (PD) marker: TMV MP-mRFP. **Figure S5.** Dynamic changes in the transcript levels of viral genes.

### Acknowledgements

We thank Dr. Michael M. Goodin (University of Kentucky, USA) for the seeds of the RFP-H2B transgenic line. We thank Dr. Yi Xu (Nanjing Agricultural University, China) for suggesting the classification of this novel virus species.

### Author contributions

FL designed the project. RQ, LG, MP, SJ, and JC conducted the experiments. All authors analyzed the data and reviewed the manuscript. RQ, FL, XZ, and WL wrote the paper. All authors read and approved the final manuscript.

### Funding

This work was supported by grants from the National Key Research and Development Program of China (2021YFD1400400) to Fangfang Li.

### Availability of data and materials

The datasets used and analyzed during the current study are available from the corresponding author at a reasonable request.

### Declarations

#### Ethics approval and consent to participate

Not applicable.

#### Consent for publication

Not applicable.

#### Competing interests

The authors declare that they have no competing interests.

Received: 2 March 2023 Accepted: 3 August 2023

Published online: 29 August 2023

### References

- Baulcombe DC. The role of viruses in identifying and analyzing RNA silencing. *Annu Rev Virol.* 2022;9(1):353–73. <https://doi.org/10.1146/annurev-virol-091919-064218>.
- Baumberger N, Tsai CH, Lie M, Havecker E, Baulcombe DC. The *Polerovirus* silencing suppressor P0 targets ARGONAUTE proteins for degradation. *Curr Biol.* 2007;17(18):1609–14. <https://doi.org/10.1016/j.cub.2007.08.039>.
- Bortolamiol D, Pazhouhandeh M, Marrocco K, Genschik P, Ziegler-Graff V. The *Polerovirus* F box protein P0 targets ARGONAUTE1 to suppress RNA silencing. *Curr Biol.* 2007;17(18):1615–21. <https://doi.org/10.1016/j.cub.2007.07.061>.
- Cai L, Dang M, Yang Y, Mei R, Li F, Tao XR, et al. Naturally occurring substitution of an amino acid in a plant virus gene-silencing suppressor enhances viral adaptation to increasing thermal stress. *PLoS Pathog.* 2023;19(4):e1011301. <https://doi.org/10.1371/journal.ppat.1011301>.
- Chen C, Du M, Peng D, Li W, Xu J, Yang XL, et al. A distinct *Tobamovirus* associated with *Trichosanthes kirilowii* mottle mosaic disease. *Front Microbiol.* 2022;13:927230. <https://doi.org/10.3389/fmicb.2022.927230>.
- Chen J, Zhao Y, Luo X, Hong H, Yang T, Huang S, et al. NLR surveillance of pathogen interference with hormone receptors induces immunity. *Nature.* 2023;613(7942):145–52. <https://doi.org/10.1038/s41586-022-05529-9>.
- Chiu KW, Davies RS, Nightingale PG, Bradbury AW, Adam DJ. Review of direct anatomical open surgical management of atherosclerotic aorto-iliac occlusive disease. *Eur J Vasc Endovasc Surg.* 2010;39(4):460–71. <https://doi.org/10.1016/j.ejvs.2009.12.014>.
- Csorba T, Lózsza R, Hutvágner G, Burgyán J. *Polerovirus* protein P0 prevents the assembly of small RNA-containing RISC complexes and leads to degradation of ARGONAUTE1. *Plant J.* 2010;62(3):463–72. <https://doi.org/10.1111/j.1365-3113x.2010.04163.x>.
- Delfosse VC, Barón M, Distéfano A. What we know about poleroviruses: advances in understanding the functions of polerovirus proteins. *Plant Pathol.* 2021;70(5):1047–61. <https://doi.org/10.1111/ppa.13368>.
- Ge LH, Cao BW, Qiao R, Cui HG, Li SF, Shan HY, et al. SUMOylation-modified Pelota-Hbs1 RNA surveillance complex restricts the infection of potyvirids in plants. *Mol Plant.* 2023;16(3):632–42. <https://doi.org/10.1016/j.molp.2022.12.024>.
- Gong P, Zhao S, Liu H, Chang Z, Li F, Zhou X. Tomato yellow leaf curl virus V3 protein traffics along microfilaments to plasmodesmata to promote virus cell-to-cell movement. *Sci China Life Sci.* 2022;65(5):1046–9. <https://doi.org/10.1007/s11427-021-2063-4>.
- Guo Z, Li Y, Ding SW. Small RNA-based antimicrobial immunity. *Nat Rev Immunol.* 2019;19(1):31–44. <https://doi.org/10.1038/s41577-018-0071-x>.
- Knierim D, Tsai WS, Deng TC, Green SK, Kenyon L. Full-length genome sequences of four polerovirus isolates infecting cucurbits in Taiwan determined from total RNA extracted from field samples. *Plant Pathol.* 2013;62(3):633–41. <https://doi.org/10.1111/j.1365-3059.2012.02653.x>.
- Kon T, Sharma P, Ikegami M. Suppressor of RNA silencing encoded by the monopartite tomato leaf curl Java begomovirus. *Arch Virol.* 2007;152(7):1273–82. <https://doi.org/10.1007/s00705-007-0957-6>.
- Koonin EV, Dolja VV. Evolution and taxonomy of positive-strand RNA viruses: implications of comparative analysis of amino acid sequences. *Crit Rev Biochem Mol Biol.* 1993;28(5):375–430. <https://doi.org/10.3109/10409239309078440>.
- Latourrette K, Holste NM, Garcia-Ruiz H. *Polerovirus* genomic variation. *Virus Evol.* 2021;7(2):102. <https://doi.org/10.1093/ve/veab102>.
- Li F, Wang A. RNA-targeted antiviral immunity: more than just RNA silencing. *Trends Microbiol.* 2019;27(9):792–805. <https://doi.org/10.1016/j.tim.2019.05.007>.
- Li F, Huang C, Li Z, Zhou XP. Suppression of RNA silencing by a plant DNA virus satellite requires a host calmodulin-like protein to repress *RDR6* expression. *PLoS Pathog.* 2014;10(2):e1003921. <https://doi.org/10.1371/journal.ppat.1003921>.
- Li F, Xu X, Huang C, Gu Z, Cao L, Hu T, et al. The AC5 protein encoded by *Mungbean yellow mosaic India virus* is a pathogenicity determinant that suppresses RNA silencing-based antiviral defenses. *New Phytol.* 2015;208(2):555–69. <https://doi.org/10.1111/nph.13473>.
- Li F, Yang X, Bisaro DM, Zhou X. The  $\beta$ C1 protein of geminivirus-betasatellite complexes: a target and repressor of host defenses. *Mol Plant.* 2018a;11(12):1424–6. <https://doi.org/10.1016/j.molp.2018.10.007>.
- Li F, Zhang C, Li Y, Wu G, Hou X, Zhou X, et al. Beclin1 restricts RNA virus infection in plants through suppression and degradation of the viral polymerase. *Nat Commun.* 2018b;9(1):1268. <https://doi.org/10.1038/s41467-018-03658-2>.
- Li S, Su X, Luo X, Zhang Y, Liu Y. First evidence showing that *Pepper vein yellows virus* P4 protein is a movement protein. *BMC Microbiol.* 2020;20(1):72. <https://doi.org/10.1186/s12866-020-01758-y>.
- Li F, Ge L, Lozano-Durán R, Zhou X. Antiviral RNAi drives host adaptation to viral infection. *Trends Microbiol.* 2022a;30(10):915–7. <https://doi.org/10.1016/j.tim.2022.07.009>.
- Li F, Qiao R, Wang Z, Yang X, Zhou X. Occurrence and distribution of geminiviruses in China. *Sci China Life Sci.* 2022b;65(8):1498–503. <https://doi.org/10.1007/s11427-022-2125-2>.
- Mayo MA, Ryabov E, Fraser G, Taliensky M. Mechanical transmission of *Potato leafroll virus*. *J Gen Virol.* 2020;81(11):2791–5. <https://doi.org/10.1099/0022-1317-81-11-2791>.
- Miller WA, Dinesh-Kumar SP, Paul CP. Luteovirus gene expression. *Crit Rev Plant Sci.* 1995;14(3):179. <https://doi.org/10.1080/07352689509701926>.
- Muhizi MB, Arvind V, Patrick M, Kuhn JH. SDT: a virus classification tool based on pairwise sequence alignment and identity calculation. *PLoS ONE.* 2014;9(9):e108277. <https://doi.org/10.1371/journal.pone.0108277>.
- Pazhouhandeh M, Dieterle M, Marrocco K, Lechner E, Berry B, Brault V, et al. F-box-like domain in the polerovirus protein P0 is required for silencing



- suppressor function. *PNAS*. 2006;103(6):1994–9. <https://doi.org/10.1073/pnas.0510784103>.
- Schoelz JE, Harries PA, Nelson RS. Intracellular transport of plant viruses: finding the door out of the cell. *Mol Plant*. 2011;4(5):813–31. <https://doi.org/10.1093/mp/sss070>.
- Shang QX, Xiang HY, Han CG, Li DW, Yu JL. Distribution and molecular diversity of three cucurbit-infecting poleroviruses in China. *Virus Res*. 2009;145(2):341–6. <https://doi.org/10.1016/j.virusres.2009.07.017>.
- Silva JMF, Al Rwahnih M, Blawid R, Nagata T, Fajardo TVM. Discovery and molecular characterization of a novel enamovirus, Grapevine enamovirus-1. *Virus Genes*. 2017;53(4):667–71. <https://doi.org/10.1007/s11262-017-1470-y>.
- Smirnova E, Firth AE, Miller WA, Scheidecker D, Brault V, Reinbold C, et al. Discovery of a small non-AUG-initiated ORF in Poleroviruses and Luteoviruses that is required for long-distance movement. *PLoS Pathog*. 2015;11(5):e1004868. <https://doi.org/10.1371/journal.ppat.1004868>.
- Sömera M, Sarmiento C, Truve E. Overview on Sobemoviruses and a proposal for the creation of the family *Sobemoviridae*. *Viruses*. 2015;7(6):3076–115. <https://doi.org/10.3390/v7062761>.
- Sömera M, Fargette D, Hébrard E, Sarmiento C, ICTV Report Consortium. ICTV virus taxonomy profile: solemoviridae 2021. *J Gen Virol*. 2021;102(12):001707. <https://doi.org/10.1099/jgv.0.001707>.
- Tamm T, Suurvälvi J, Lucchesi J, Olsper A, Truve E. Stem-loop structure of *Cocksfoot mottle virus* RNA is indispensable for programmed-1 ribosomal frameshifting. *Virus Res*. 2009;146(1–2):73–80. <https://doi.org/10.1016/j.virusres.2009.09.002>.
- Tan ST, Liu F, Lv J, Liu QL, Luo HM, Xu Y, et al. Identification of two novel poleroviruses and the occurrence of Tobacco bushy top disease causal agents in natural plants. *Sci Rep*. 2021;11(1):21045. <https://doi.org/10.1038/s41598-021-99320-x>.
- Thordal-Christensen H, Zhang Z, Wei Y, Collinge DB. Subcellular localization of H<sub>2</sub>O<sub>2</sub> in plants. H<sub>2</sub>O<sub>2</sub> accumulation in papillae and hypersensitive response during the barley—powdery mildew interaction. *Plant J*. 1997;11(6):1187–94. <https://doi.org/10.1046/j.1365-313X.1997.11061187.x>.
- Walker PJ, Siddell SG, Lefkowitz EJ, Mushegian AR, Adriaenssens EM. Changes to virus taxonomy and to the international code of virus classification and nomenclature ratified by the International Committee on Taxonomy of Viruses. *Arch Virol*. 2021;166(9):2633–48. <https://doi.org/10.1007/s00705-021-05156-1>.
- Wang JY, Chay C, Gildow F, Gray SM. Readthrough protein associated with virions of barley yellow dwarf luteovirus and its potential role in regulating the efficiency of aphid transmission. *Virology*. 1995;206(2):954–62. <https://doi.org/10.1006/VIRO.1995.1018>.
- Wang L, Tian P, Yang X, Zhou X, Zhang S, Li C, et al. Key amino acids for *Pepper vein yellows virus* P0 protein pathogenicity, gene silencing, and subcellular localization. *Front Microbiol*. 2021;12:680658. <https://doi.org/10.3389/fmicb.2021.680658>.
- Wang KD, Dughbaj MA, Nguyen TTV, Nguyen TQY, Oza S, Valdez K, et al. Systematic mutagenesis of *Polerovirus* protein P0 reveals distinct and overlapping amino acid functions in *Nicotiana glutinosa*. *Virology*. 2023;578:24–34. <https://doi.org/10.1016/j.virol.2022.11.005>.
- Wilk F, Verbeek M, Dullemans AM, van den Heuvel J. The genome-linked protein of potato leafroll virus is located downstream of the putative protease domain of the ORF1 product. *Virology*. 1997;234(2):300–3. <https://doi.org/10.1006/VIRO.1997.8654>.
- Wu JX, Zhou XP. Production and application of monoclonal antibodies against Potato virus X. *J Zhejiang Univ B*. 2015;31:608–12. <https://doi.org/10.1046/j.1365-3059.1998.00238.x>.
- Wu JX, Shang HL, Xie Y, Shen QT, Zhou XP. Monoclonal antibodies against the whitefly-transmitted *Tomato yellow leaf curl virus* and their application in virus detection. *J Integr Agric*. 2012;11(2):263–8. [https://doi.org/10.1016/S2095-3119\(12\)60010-0](https://doi.org/10.1016/S2095-3119(12)60010-0).
- Xiang HY, Shang QX, Han CG, Li DW, Yu JL. Complete sequence analysis reveals two distinct poleroviruses infecting cucurbits in China. *Arch Virol*. 2008;153(6):1155–60. <https://doi.org/10.1007/s00705-008-0083-0>.
- Xu Y, Ju HJ, DeBlasio AS, Carino BEJ, Johnson R, et al. A stem-loop structure in *Potato leafroll virus* open reading frame 5 (ORF5) is essential for readthrough translation of the coat protein ORF stop codon 700 bases upstream. *J Virol*. 2018;92(11):e01544–e1617. <https://doi.org/10.1128/jvi.01544-17>.
- Yang Z, Li Y. Dissection of RNAi-based antiviral immunity in plants. *Curr Opin Virol*. 2018;32:88–99. <https://doi.org/10.1016/j.coviro.2018.08.003>.
- Yang M, Liu Y. Autophagy in plant viral infection. *FEBS Lett*. 2022;596(17):2152–62. <https://doi.org/10.1146/annurev-virology-010220-054709>.
- Yang Z, Huang Y, Yang J, Yao S, Zhao K, Wang D, et al. Jasmonate signaling enhances RNA silencing and antiviral defense in rice. *Cell Host Microbe*. 2020;28(1):89–103.e8. <https://doi.org/10.1016/j.chom.2020.05.001>.
- Zhang M, Cao B, Zhang H, Fan Z, Zhou X, Li F. Geminivirus satellite-encoded βC1 activates UPR, induces bZIP60 nuclear export, and manipulates the expression of bZIP60 downstream genes to benefit virus infection. *Sci China Life Sci*. 2023;66(6):1408–25. <https://doi.org/10.1007/s11427-022-2196-y>.

Ready to submit your research? Choose BMC and benefit from:

- fast, convenient online submission
- thorough peer review by experienced researchers in your field
- rapid publication on acceptance
- support for research data, including large and complex data types
- gold Open Access which fosters wider collaboration and increased citations
- maximum visibility for your research: over 100M website views per year

At BMC, research is always in progress.

Learn more [biomedcentral.com/submissions](https://biomedcentral.com/submissions)

